SVU-International Journal of Engineering Sciences and Applications (2022) 3(1): 64-77
Print ISSN 2785-9967 | Online ISSN 2735-4571
DOI 10.21608/svusrc.2022.132207.1044

Procedural Framework for Assessing the Impact of New Cities Growth on Urban Heat Island, A Case Study of 6thOctober City

Zeinab A. Alsonny [1], Omar Hamdy [2]
1-https://orcid.org/0000-0002-6812-403X.
2-https://orcid.org/0000-0002-7379-9461.

Abstract In order to control urban growth, Egypt resorted to establishing new cities on the boundaries of existing ones. Thus, there is concern that the urban heat island phenomenon (UHI) will increase in these desert cities as their urban growth This phenomenon is dependent on land surface temperatures (LST), which are difficult to measure over large areas in situ. As a result, this research is focused on two primary objectives. The first objective is to establish a framework for examining the relationship between urban growth and LST over time using freely available data from remote sensing (RS) and geographic information systems (GIS). The second objective is to validate and apply this framework in order to ascertain the impact of changes in urban growth on the LST of 6th of October City, which will serve as a case study for new cities. Satellite images for the years 2001, 2007, 2013, and 2019 were obtained using the Landsat data source. Hence, the Land Use/Land Cover Classification (LULC) was obtained with excellent Kappa values of 0.973, 0.962, 0.962, and 0.968, respectively. By examining the relationship between LST and urban growth, the framework was able to produce satisfactory results regarding the impact of urban growth on UHI. It was discovered that as urbanization increases, the city's average LST decreases. This is because it increases the likelihood of shading and the presence of green spaces, rather than desert areas that absorb the most radiation. Thus, urbanization does not endanger UHI in new cities.

Keywords:. Urban Heat Island; Remote Sensing; Urban Growth; LULC; GIS; LST.

1 Introduction

Egypt, like a large number of developing countries, is confronted with issues related to urban sprawl. Despite the government's efforts to limit the pace of urban growth during the last five decades, there has been an unprecedented rate of urban expansion. Because the growth of urban areas depends on the population growth [1] it can be observed that, Urban population accounted for less than 10% of the overall population at the turn of the twentieth century [2], but had increased by 45% at the century's end. The urban population is anticipated to rise at a pace of 2.2 % per year through 2050, significantly faster than the overall Egyptian population's yearly growth rate of 1.8 percent [3]. Hence the need to create new cities to accommodate the increasing urban growth [4]. The most notable feature of these new settlements is their location in desert areas [5], which raises concerns about rising temperatures in these places.

There is no doubt that urban growth and industrialization have improved our material life and our comfort. However, surface modifications induced by urban growth also causes many problems because of its significant impact on the natural environment [6] and the occurrence of the urban heat island (UHI) phenomenon [7]. The UHI phenomenon is one of the most important factors affecting the urban climate [8]. It is defined as an increase in air and surface temperatures in cities compared to rural areas [9], [10]. This local temperature difference caused by UHI has a negative impact on humans and the environment because it impairs air quality, increases energy consumption [7]. One of the most serious consequences of UHI is that thermal comfort is adversely affected [8]. Heat stress resulting from high temperatures has the effect of increasing economic stress, especially in developing countries [11].

Land surface temperature (LST) measurement is critical

Received: 8 April 2022/ Accepted: 24 April 2022
Corresponding Author, Omar Hamdy,
Email: omar.hamdy@aswu.edu.eg
[1,2] Architectural Engineering Department, Aswan University, Egypt.

to UHI studies. LST is a key variable in interactions and energy flows between the Earth's surface and the atmosphere [12]. It has to do with surface radiation, the internal climate of buildings, and human comfort in cities [13]. LST directly interacts with Land Use /Land Cover (LULC) characteristics of an area [14]. The relationship between LULC and LST is critical to understanding the effects of LULC on UHI [7]. Owing to the complexity of LST measurement, ground measurements cannot provide LST values over large areas and are, moreover, time-consuming and expensive. Satellite remote sensing (RS) provides free, easily accessible, continuous and spatially distributed data at different time periods, thus giving researchers the opportunity to further understand the complex relationship between the spatio-temporal variability of surface thermal conditions and their driving factors [12].

Among the satellites, the Landsat series of satellites has a long history of freely available archival data dating back to 1972 [11], making it suitable for studying the UHI in earlier years. According to meteorological records, we find that 2007 and 2013 were the sixth warmest years since the beginning of world records in 1850 [15]. They were determined as years of study in addition to the year before them and the year after them for the same period of time. So, the study years are as follows: 2001, 2007, 2013, 2019. Satellite data are analyzed by geographic information systems (GIS), which have proven efficiency in scientific research [16]. The integration of RS and GIS helps improve accuracy as well reduce mapping cost [17] and provides a strong and complementary set of approaches for monitoring the urban growth [1][18].

The availability of free data has enabled researchers in developing countries to study many of the problems of urban growth. Which otherwise would not have been possible due to financial constraints. Therefore, the study aims to achieve two main objectives. The first objective is to formulate a framework using freely available data based on RS and GIS that planners in developing countries can use to analyze the impact of urban growth on the UHI of cities. The second objective is to apply and test this framework using it to determine the urban growth and LST of 6th of October City as a case study of being one of the first new cities to be established in Egypt. Because the more the new city progresses, the more local infrastructure and facilities are planned and implemented [19].

2 Martial and Methods

2.1 The Study Area

The study was conducted on 6th October City, which is one of the most important cities in Egypt's first generation of new cities (**Fig. 1**). It was established in 1979. The city is known for its superb location - east of Cairo and north of the pyramids. The entrances to the city are defined by the Dabaa axis in the north, Al-Wahat Road, the Middle Ring Road in the east, Fayoum Road in the south, and the Regional Ring Road in the west. Astronomically, the city lies between latitudes N30°03'23.04" and N29°52'35.04" and longitudes E31°05'9.6" and E30°47'26.88". With a total area of 55 thousand acres [20]. 6th October City serves as a model for land use efficiency, having abided by the principles of optimal use and diversity of use [21]. Which makes the city suitable for conducting the study on it.

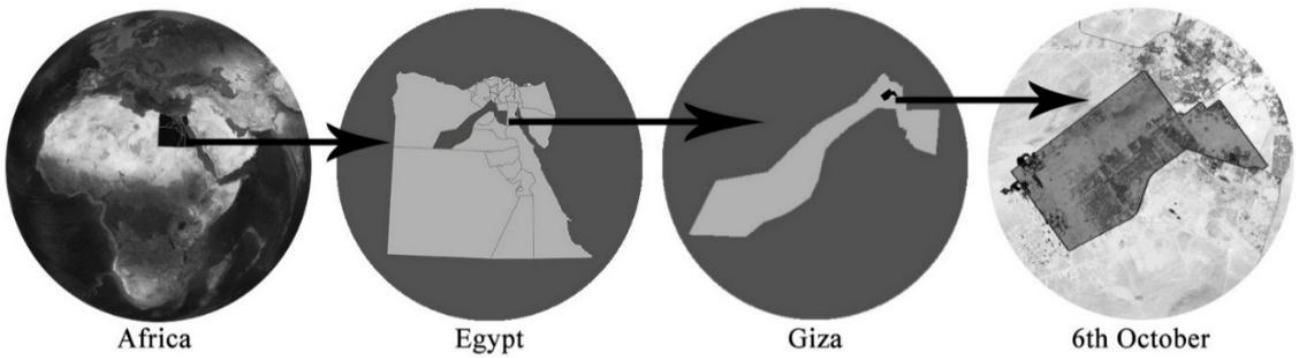

Fig. 1 The study area location

2.2 Research methodology

Many methods have been used to reach the desired goals. The inductive method was used to collect data about the city, obtain the necessary maps and coordinates, and select the appropriate satellites from which to take images for the study. In the applied approach, the remote sensing (RS) data was processed using geographic information systems (GIS). The land surface temperatures (LST) extraction equations were applied to satellite images and the resulting temperatures were assigned to different categories. Satellite images were also classified for Land Use /Land Cover (LULC). Finally, the analytical approach was used to analyze the relationship between LST and LULC to understand the effect of urban growth on urban heat island phenomenon (UHI) (**Fig. 2**). It will also be explained in detail.

2.2.1 Data collection and visual processing

At this important stage, relevant data concerning 6th October City up to its outer limits were collected. The date of the visual capture and RS applications data were collected and differentiated between satellites. Landsat 8, the newest satellite, was chosen to capture satellite images for 2019 and 2013. As Landsat 7 images had malfunctions, Landsat 5 images for 2007 and 2001 were chosen instead. Since there were daily temperature variations depending on the weather, three satellite images were selected for each year of the study. UHI is clear in summer owing to strong radiation [22], so satellite images during summer were used. Although summer begins astronomically on June 21 and ends on September 23, it can be divided into three months and phases based on human observations as follows:

- Regular summer phase from June 7 to July 6: It is usually the lightest summer. The weather is hot during the day, the nights tend to be moderate, and the weather is dry.
- Dry heat phase from July 7 to August 6: The weather is very hot, summer rain is heavy, and homes are very hot.
- Wet heat phase from August 7 to September 6: The weather is very hot during the day, and the nights tend to be hot too, but temperatures are lower than during the dry heat phase. Chances of rain are higher.

Satellite data were collected from the USGS website: https://earthexplorer.usgs.gov/ [23]; satellite images were captured in each of the summer months of the study years (2001-2007-2013-2019) as shown in **Table 1**.

Table 1 Dates of satellite images

Years of study	Satellite	1st Group	2nd Group	3rd Group
2001	Landsat 5	24-6-001	26-7-001	27-8-001
2007	Landsat 5	25-6-007	27-7-007	28-8-007
2013	Landsat 8	25-6-013	27-7-013	28-8-013
2019	Landsat 8	26-6-019	28-7-019	29-8-019

2.2.2 RS Data Processing

2.2.2.1 LULC classification

The classification process begins with incorporating all bands, except for thermal bands 10 and 11 in Landsat 8, and Band 6 in Landsat 5 because they measured the radiant energy emitted by the infrared rays of the Earth's surface. The 8-Panchromatic band was also excluded. Then, the study area was subtracted from the final image. The bands were arranged to show the image in natural colors without the atmosphere. LULC training samples were taken from the satellite image and a signature file was created for them. Depending on the signature file, the supervised classification was performed using the maximum likelihood classification method. It is one of the most important controlled classification methods widely used in LULC mapping [17][24].

2.2.2.2 LULC classification accuracy validation

The classification processes is subjected to the classification accuracy assessment process which is a necessary stage to assess the quality of the maps obtained from RS data [25]. The methods for assessing the accuracy of classification in the field are expensive and time-consuming because they are based on the use of GPS and high-resolution images that may not be available [26]. Therefore, an error matrix was used, which is the most common way to present the accuracy of the classification results [14][27].

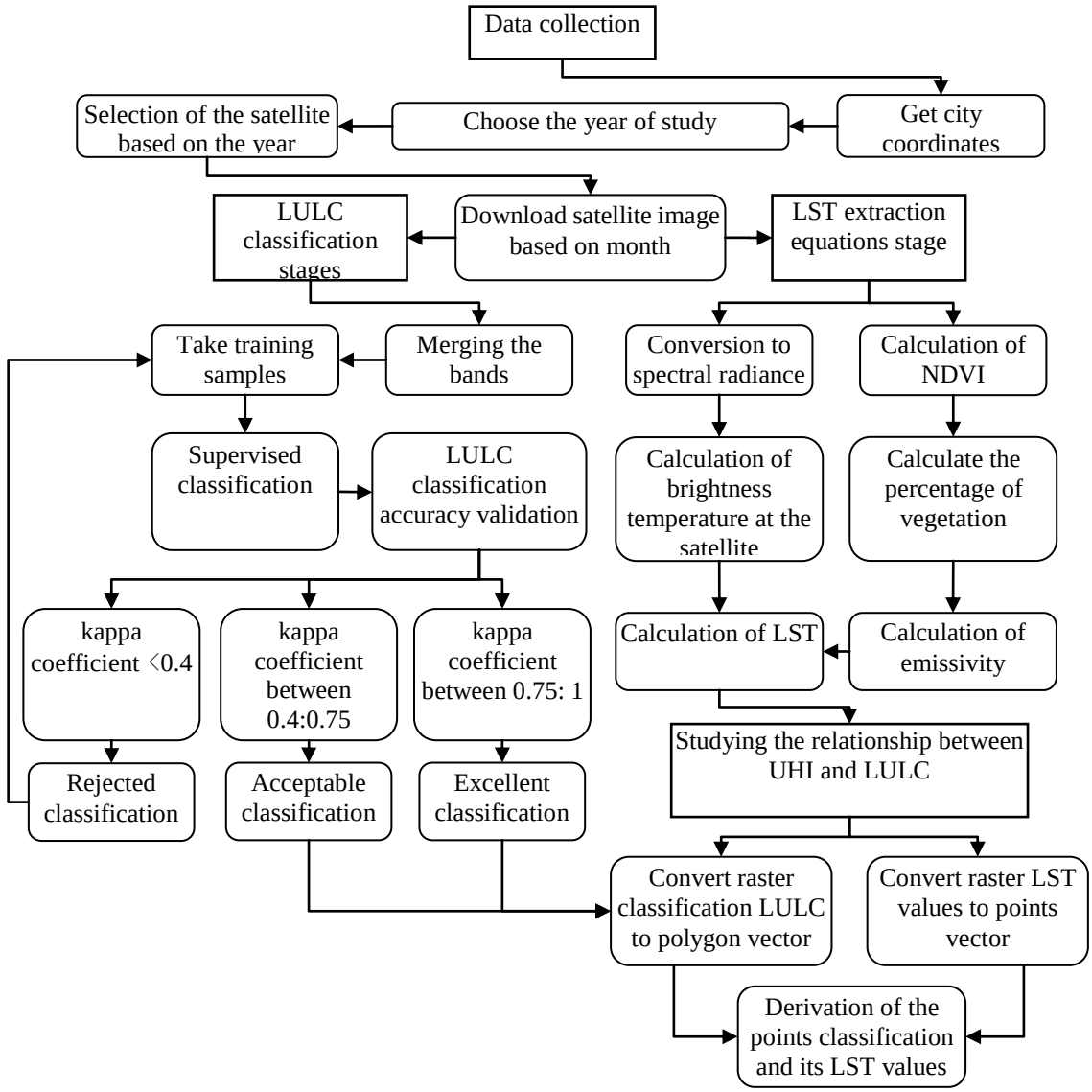

Fig. 2 Diagram showing the framework of the research methodology

It is based on a set of samples obtained from a valid reference classification such as Google Earth. It is recommended that samples be between 50 to 100 samples for each category of classification to ensure acceptable accuracy [26]. The kappa coefficient was calculated, which is one of the frequently used variables in error matrix analyzes [25]. The kappa coefficient ranges from 0 to 1, and the closer its value is to 1, the higher the classification accuracy. Studies have shown that a kappa value between 0.75 to 1 indicates excellent accuracy, while a value between 0.4 to 0.75 indicates good accuracy, and a value less than 0.40 indicates poor accuracy results [28].

2.2.2.3 LST extraction equations

This stage relied on the application of several important equations that are dependent on each other for the calculation of LST. They were collected from previous studies. These equations were applied to the heat bands (band 6 for Landsat 5 and bands 10, 11 for Landsat 8) using ArcGIS 10.5, as shown below:

2.2.2.3.1 Conversion to spectral radiance:

Landsat 8's algorithms for converting digital number (DN) to spectral radiance were different from those used by prior Landsat satellites. The following is the equation for the Landsat 8 satellite:[29] [30]; [31]

$$L\lambda = ML * Qcal + AL \quad (1)$$

Where: Lλ = Spectral Radiance at the sensor's aperture, ML = Band-specific multiplicative rescaling factor from the metadata, AL= Band-specific additive rescaling factor from the metadata, Qcal = Quantized calibrated pixel value in DNs.

The equation for the Landsat 5 satellite is as follows: [32]

$$L\lambda = \left((LMAX\lambda - LMIN\lambda)/(QCALMAX - QCALMIN)\right) * (QCAL - QCALMIN) + LMIN \quad (2)$$

Where: Lλ = Spectral Radiance at the sensor's aperture, LMAXλ = Maximum spectral radiance at QCAL (from metadata files), LMINλ= Minimum spectral radiance at QCAL (from metadata files), QCALMAX = Maximum quantized calibrated pixel value (corresponding to LMAXλ) in DN 255 (from metadata files), QCALMIN= Minimum quantized calibrated pixel value (corresponding to LMINλ) in DN 0 or 1 (from metadata files), QCAL= Quantized calibrated pixel value in DNs.

2.2.2.3.2 Calculation of brightness temperature at the satellite:

The following equation was used to calculate the brightness temperature or black body temperature at the satellite: [11]

$$T_{(K)} = \frac{K2}{\ln\left(\frac{K1}{L\lambda} + 1\right)} \quad (3)$$

Where: T(K)= Temperature in kelvins, Lλ= Spectral Radiance at the sensor's aperture, K1, K2= Calibration constants (from metadata files). Its values changed according to the satellite as shown in **Table 2**.

Table 2 Values of k . constant

	Satellite	K1	K2
Landsat 5	Band 6	607.76	1260.56
Landsat 8	Band 10	774.8853	1321.0789
	Band 11	480.8883	1201.1442

The temperature was converted to Celsius degrees from the following equation: [33]

$$T_{(°C)} = T_{(K)} - 273.15 \quad (4)$$

2.2.2.3.3 Calculation of the Normalized Difference Vegetation Index (NDVI):

LST was based on the calculation of the NDVI for both Landsat 8 and Landsat 5 images through the following equation: [32]

$$NDVI = (\text{NIR} - \text{RED})/(\text{NIR} + \text{RED}) \quad (5)$$

Where: NIR= Near infrared bands, RED= Visible infrared bands. So, the equation for the Landsat 8 satellite is as follows: [34]

$$NDVI = (Band5 - \text{Band4})/(Band5 + Band4) \quad (6)$$

And the equation for the Landsat 5 satellite is as follows: [32]

$$NDVI = (Band4 - Band3)/(Band4 + Band3) \quad (7)$$

Then, the study area was extracted from the resulting digital image of NDVI.

2.2.2.3.4 Calculation of the percentage of vegetation

Vegetation was calculated by the following equation: [35]

$$P_V = \left(\frac{NDVI - NDVI_{MIN}}{NDVI_{MAX} - NDVI_{MIN}}\right)^2 \quad (8)$$

Where: Pv = Percentage of vegetation, NDVImin =Minimum value of NDVI, NDVImax =Maximum value of NDVI.

2.2.2.3.5 Calculation of emissivity:

Emissivity was calculated given the percentage of vegetation cover by the following equation: [30]

$$\varepsilon = 0.004P_V + 0.986 \quad (9)$$

2.2.2.3.6 Calculation of LST:

The following equation was used to compute LST in Celsius based on NDVI, black body temperature at the sensor, and emissivity (all of which had already been calculated): [32]; [30]

$$LST = \frac{T(°C)}{1+\left(\frac{LA \cdot T(°C)}{\rho}\right) \cdot \ln(\varepsilon)} \quad (10)$$

Where: ρ =Constant value $= h * \frac{c}{\sigma} = (1.438 * 10^{-2} m * K)$. It is worth noting that after obtaining the LST, it was divided into several categories, with one degree Celsius separating each category.

2.2.3 Evaluating the relationship between UHI and LULC:

The LST categories in the study area were distributed on the LULC classification. The temperature changes of LULC classifications at different time intervals were studied to determine how urban growth affected the LST mean of the city.

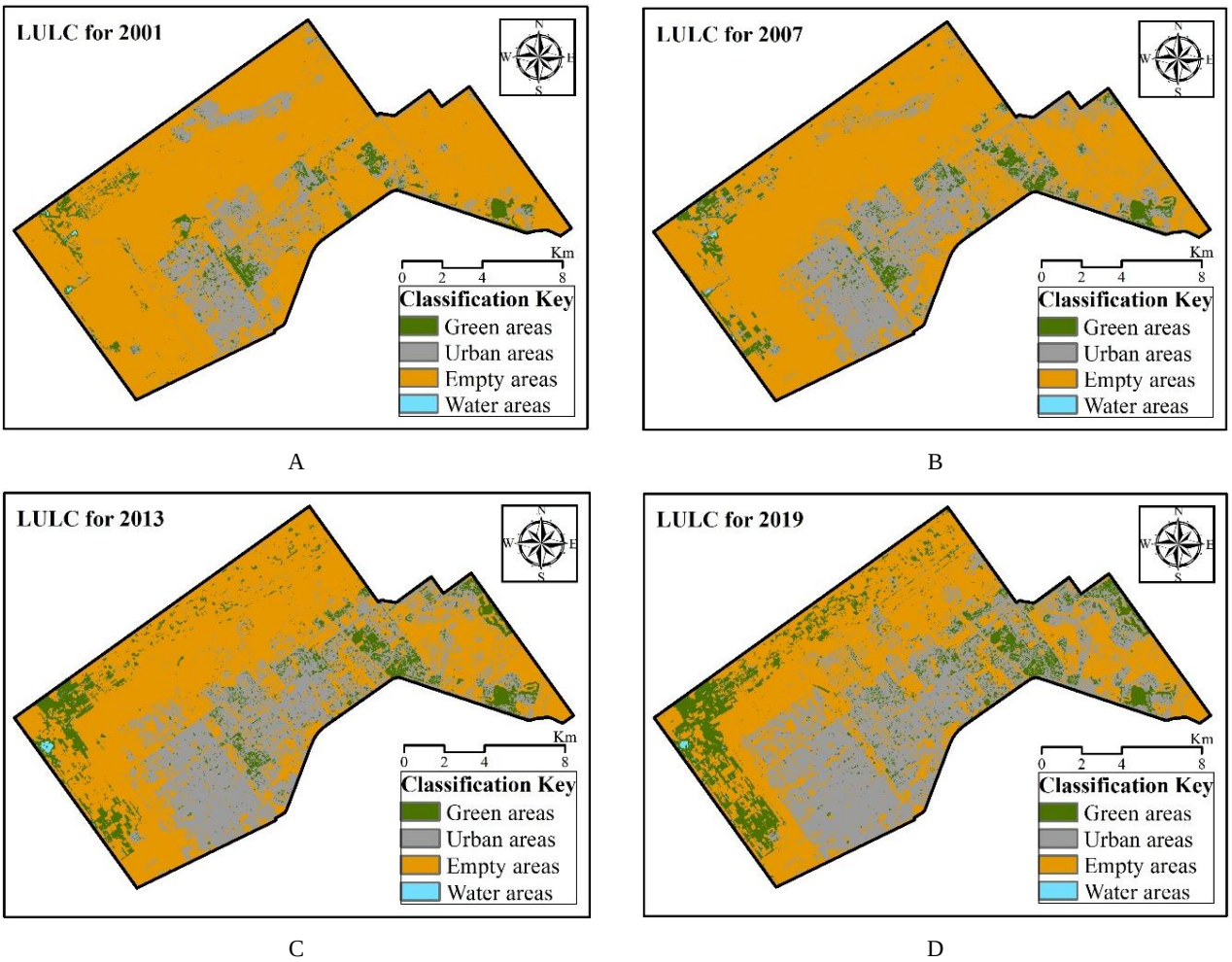

Fig. 3 LULC classification for 6th October City through the study years

3 Results and discussion

3.1 Land use classification

LULC for 6th of October City was classified into four categories, viz. urban, green, water, and empty areas. As shown in **Fig. 3**, urban areas were growing significantly, as were green areas and water areas, while empty areas decreased between 2001 and 2019. The statistics showed that empty, urban, green and water areas were 79.8%, 15.3%, 4.8%, and .07% respectively of the city's total area in 2001. The proportions of these areas in relation to the total area of the city changed in 2007 to 70.1%, 23.7%, 6.04%, .08% respectively; in 2013, the areas were 60.30%, 29.51%, 10.08%, .11% respectively; and in 2019 the areas were 49.22%, 37.36%, 13.37%, .06%, respectively of the total city area. By comparing these areas during the study

years from 2001 to 2019, it appears that empty and water areas were decreasing and that urban and green areas were expanding, as shown in **Fig. 4**.

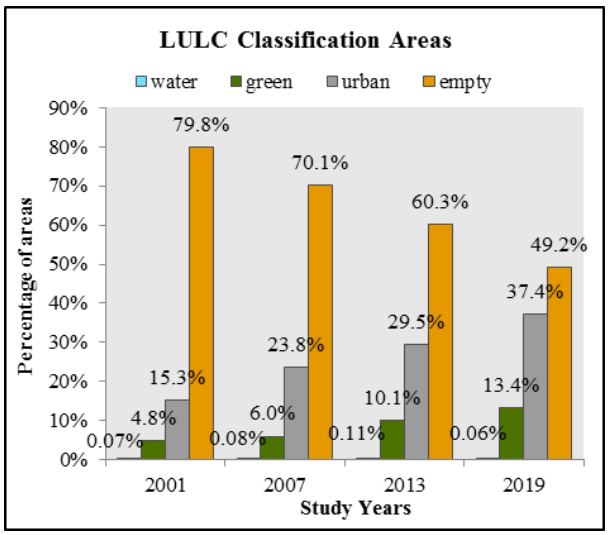

Fig. 4 LULC classification percentage through the study years.

3.2 Urban Growth

In 2001, the urban areas looked modest compared to surrounding non-urban areas, but by 2019, this area had doubled to cover the majority of the land in the city (**Fig. 5**). We note that there was an error rate in the classification. Some areas were classified as urban in 2001 and 2007, but in later years, they were classified differently. Most of these areas are in the northern region which is designated as a green belt. In light of this urban expansion, it is illogical to have urban areas classified differently later. These areas were, therefore, deemed to have been misclassified. The error rate was determined for each year of study in relation to the current year (**Fig. 6**). The error rate for 2019 was not determined because it was the last year covered in the study, and no newer classification was available to check whether or not it was in the urban areas that were misclassified.

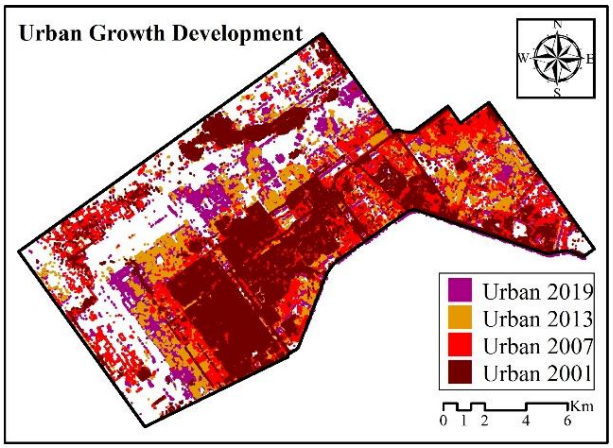

Fig. 5 Comparison of the urban growth development through the study years.

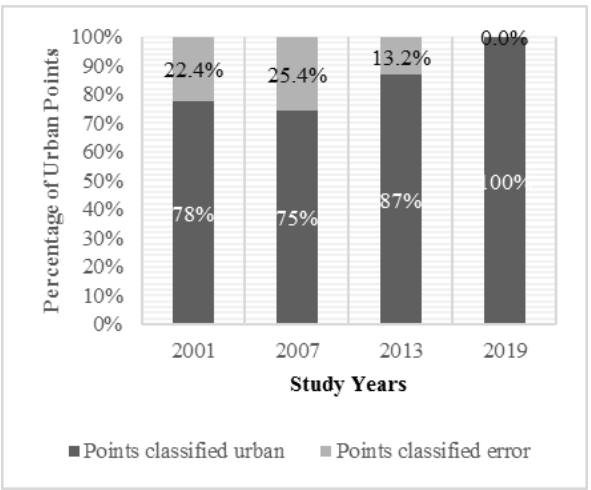

Fig. 6 The percentage of error in the classification of urban areas.

3.3 Accuracy Assessment (Kappa Coefficient)

Two hundred and fifty samples were taken to assess the classification accuracy for each year of study. The samples were distributed among the different LULC classifications (50 – 100 samples each) according to their areas. Error matrices were generated and the kappa coefficients were calculated. The kappa values show that the classifications were accurate. The kappa coefficient in 2001 was 0.973, while in 2007 and 2013 it was 0.962. In 2019, the kappa coefficient was 0.968. Therefore, all the LULC classifications were considered to have excellent accuracy.

3.4 Comparison of summer LST in the study years

In 2001, LST was low at the beginning of summer. It ranged from about 23.7° to 38°. The beginning of the

summer of 2007 had moderate LST, with areas experiencing temperatures between 36° to 40°. the summer in 2013 started with high LST over a wide area. The temperatures were in the range of 41°to 47° in some areas. While the beginning of summer 2019 was mild, with many areas experiencing temperatures in the 34° to 39° range, a few areas were much warmer, with LST soaring to 45° as shown in **Fig. 7**.

Fig. 8 shows that LST increased in midsummer 2001 to nearly 43° in some areas as shown in Figure 12. LST increased in midsummer 2007, and most areas had temperatures in the range of 41° to 47°. Midsummer 2013 LST was lower, with many areas experiencing temperatures ranging from 34 ° to 40 °. In mid-summer 2019, LST rose in mid-summer 2019. LST in many areas tended to rise from 41° to 46° in some areas.

LST rose at the end of summer 2001, ranging from 43° to 51°. LST dropped significantly at the end of summer 2007, with many areas having temperatures between 26° and 31°. The end of the summer of 2013 saw cooler temperatures than at the beginning of summer, with LST ranging between 27° to 42 °. LST dropped dramatically at the end of summer 2019. LST in most areas ranged from 28° to 38°. Some areas exceed this limit, reaching a maximum of about 43° as shown in **Fig. 9**.

A comparison of the beginning of summer (the usual summer phase) in each year of the research reveals that the beginning of the summer in 2013 was the warmest, while the beginning of the summer of 2001 was the least warm, as shown in **Fig. 7**. While **Fig. 8** shows that LST was quite similar in the middle of summer (dry heat phase) in each of the study years, the hottest was the middle of summer in 2007. Although the LST for the end of summer (wet weather heat phase) in each of the study years was relatively similar, the end of the summer of 2001 was hotter, as shown in **Fig. 9**. A comparison of LST mean for summer in each of the study years shows that LST for 2007 and 2013 was higher than for other years (see **Fig. 10**). A higher LST also meant a higher UHI for these two years.

3.5 Relationship between LULC classification and LST for the city

3.5.1 Distribution of LST categories on LULC classifications

The LULC classification was distributed over the temperature classes for each year of study as shown in **Table 3**. We note that in 2001, the highest percentage grouped into one category, which was approximately 30% of the total empty spaces, was within the category of 38°-39°. The highest percentage of urban and green areas, which were 29.1% and 15.2% respectively, fell within the 36°-37° category. The highest percentage of water areas was 48.9%, and it was in the category below 29° degrees. This value changed slightly in 2007 to become the highest percentage of vacant areas within the category of 39°- 40° while the highest percentage of urban and green areas were within the category of 38°-39°.

In 2013 the highest percentage of vacant and urban areas remained unchanged but the highest percentage of green spaces fell into the category of 35°-36°. In 2019 the highest percentage of empty and green spaces fell into the category of 39°-40° but the highest percentage of urban areas fell into the category of 37°-38° (**Fig. 11**).

Empty areas are devoid of shade, and thus they are exposed to the greatest amount of solar radiation. It is, therefore, not surprising that the empty areas fell into categories with high temperatures. The highest percentages of urban and green areas fell into categories with a similar temperature range, thus both urban and green areas were intertwined. The presence of green areas permeating urban areas, in addition to the presence of shade, led to significantly moderate temperatures in these areas. We note that the water areas fell into the category of lowest temperatures.

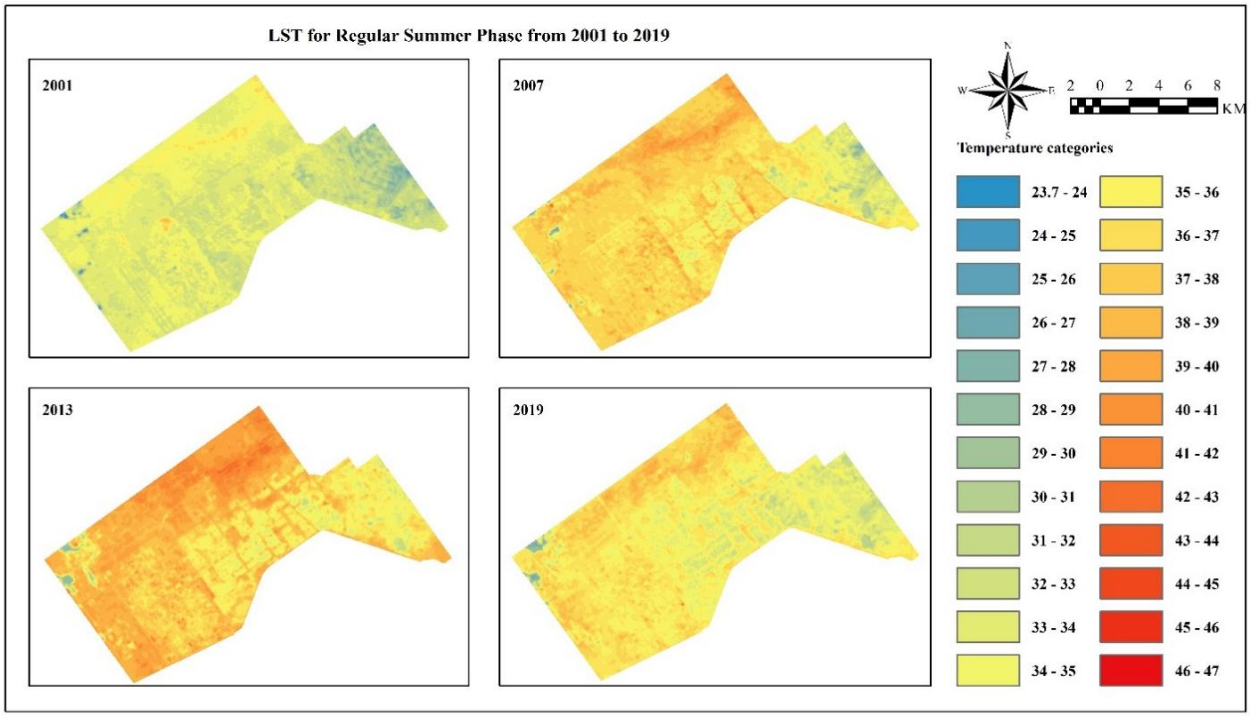

Fig. 7 Comparison of the regular summer phase over the study years.

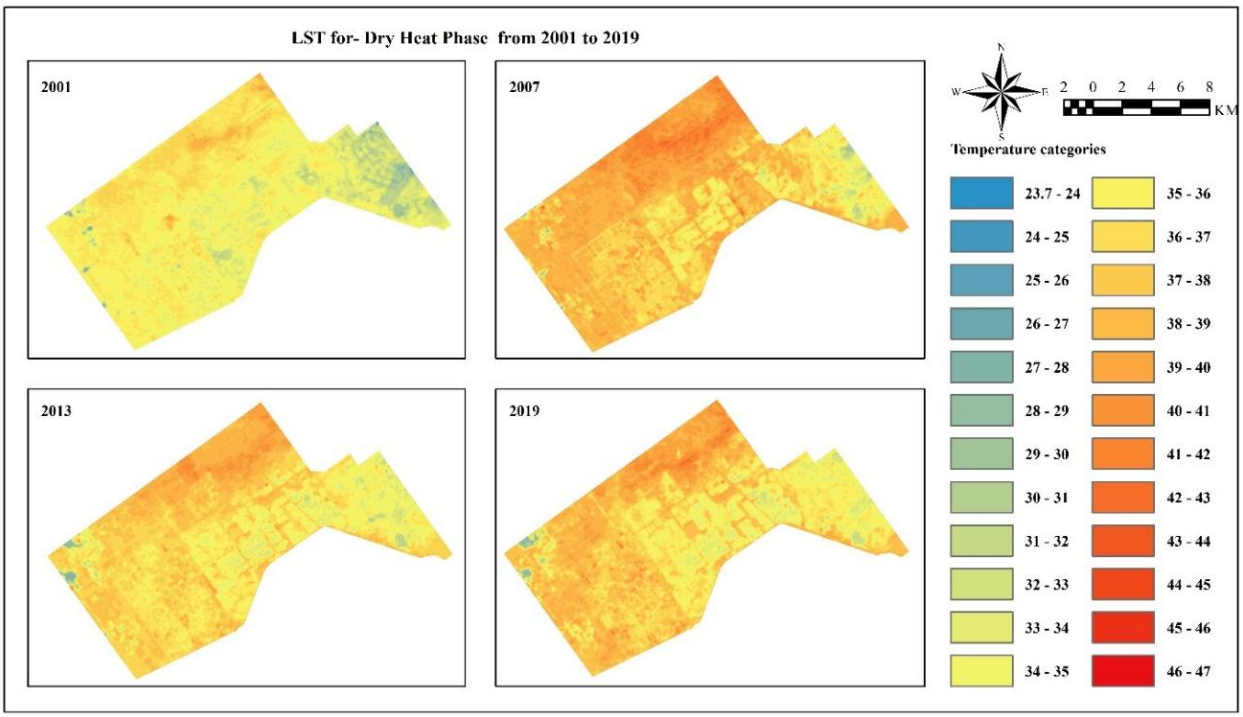

Fig. 8 Comparison for the dry heat phase over the study years.

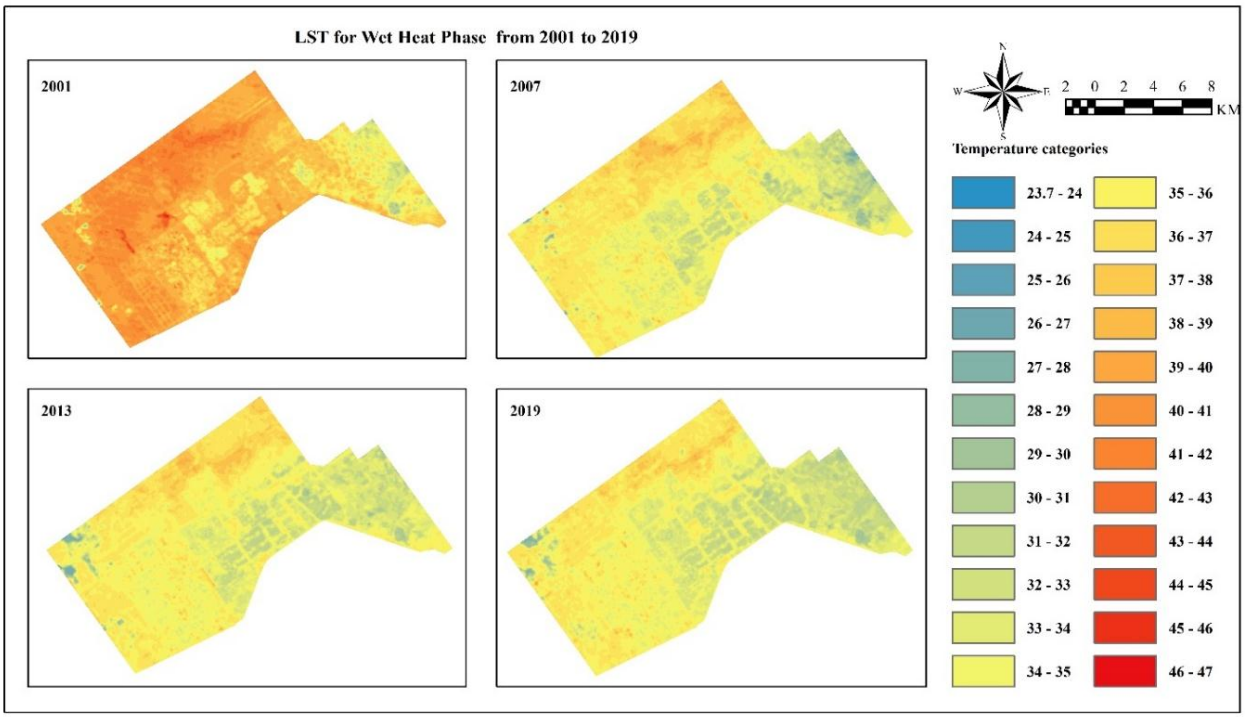

Fig. 9 Comparison for the wet heat phase over the study years.

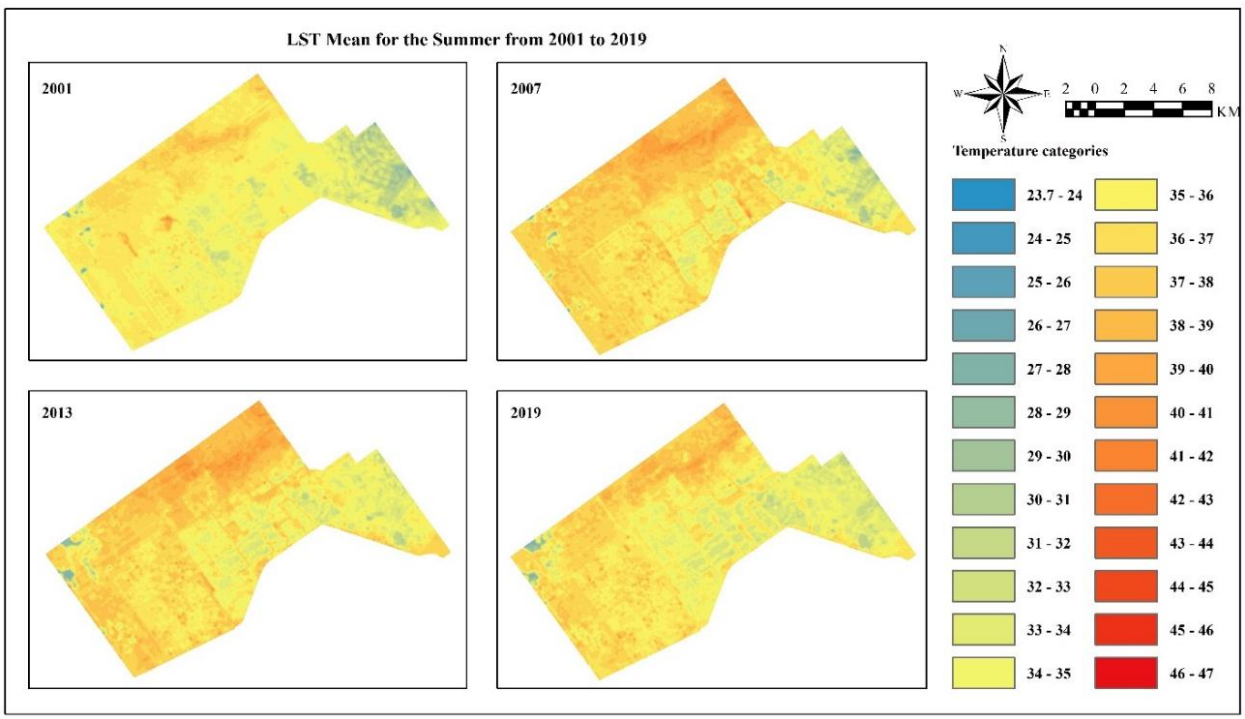

Fig. 10 Comparison of LST mean every seventh year during the study period.

Table 3 shows the highest percentage of classification for the count of points in the classification for each year and its temperature category.

	2001		2007		2013		2019	
	The highest percentage	Category	The highest percentage	Category	The highest percentage	Category	The highest percentage	Category
Empty areas	30.68%	38-39	34.5%	40-39	30.0%	40-39	30.1%	40-39
Urban areas	29.1%	37-36	24.8%	39-38	22.7%	39-38	21.3%	38-37
Green areas	15.2%	37-36	16.6%	37-36	16.5%	36-35	17.0%	40-39
Water areas	48.9%	29>	25.7%	29>	74.7%	29>	53.8%	29>

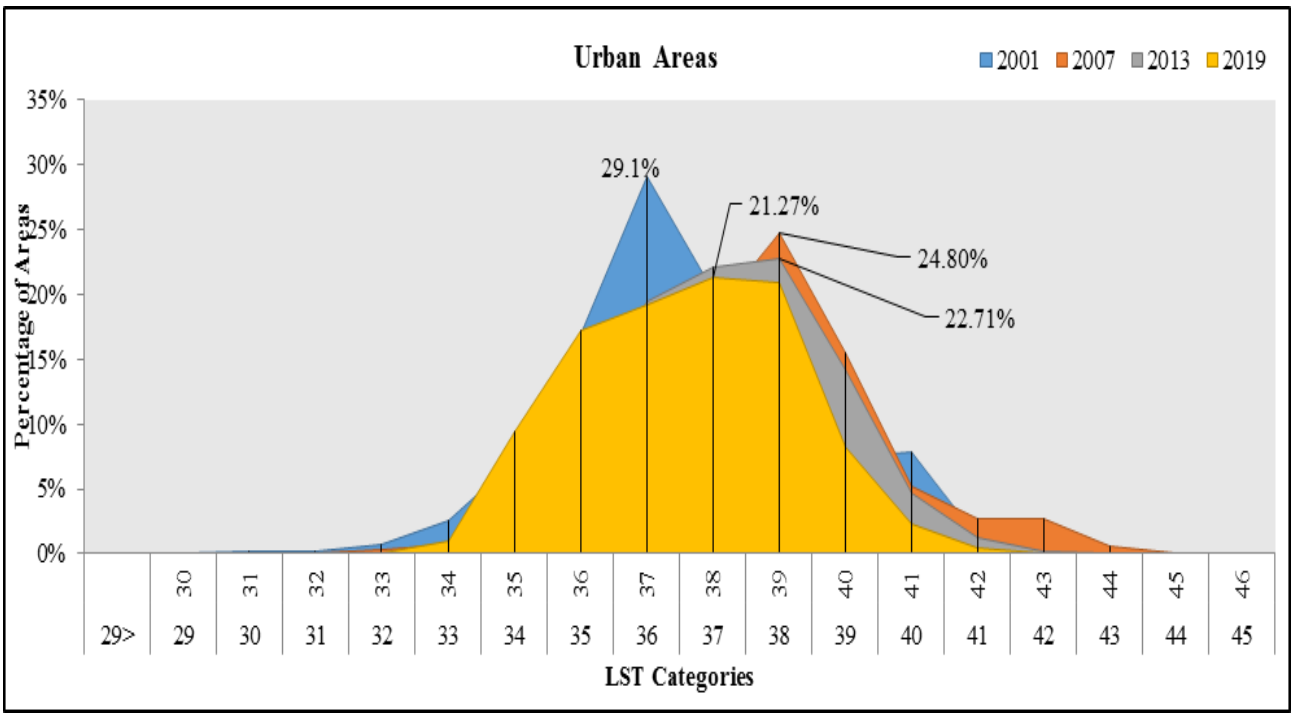

Fig. 11 Distribution of LST categories on LULC classifications for the years of study.

3.5.2 Relationship between urban areas and LST

The impact of urban growth on UHI is illustrated by examining the relationship between urban growth and the LST mean of a city as shown in **Table 4**. In 2001, the built-up area was equivalent to 40% of the urban area in 2019. The LST mean of the urban area and the LST mean of the entire city within its boundaries in that year were 36.96° and 37.21° respectively. The built-up area in 2007 was the equivalent of 62.8% of the urban area in 2019. The LST mean of the urban area and the LST mean of the entire city was 37.97° and 38.75°, respectively. In 2013, the urban area was equivalent to 78.7% of that in 2019, with the LST mean in these urban areas at 37.66°, while the LST mean of the entire city was 38.63°. Urban areas increased until the area reached approximately 20,045.47 acres in 2019, with the LST mean in these urban areas at 37.10°, while the LST mean of the entire city was 37.83° as shown in **Fig. 12** and **Fig. 13**.

Table 4 The relationship of urban development to their LST mean for the years of study

Years of study	2001	2007	2013	2019
Urban Area (Acre)	8148	12582	15778	20045
Percentage for the current urban (2019)	40.6%	62.8%	78.7%	100.0%
LST mean of urban	36.96°	37.97°	37.66°	37.10°
LST mean for total city	37.21°	38.75°	38.63°	37.83°

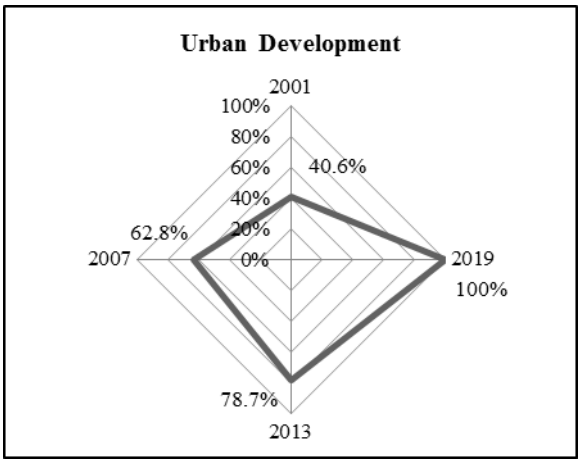

Fig. 12 The growth of urban areas during the study years.

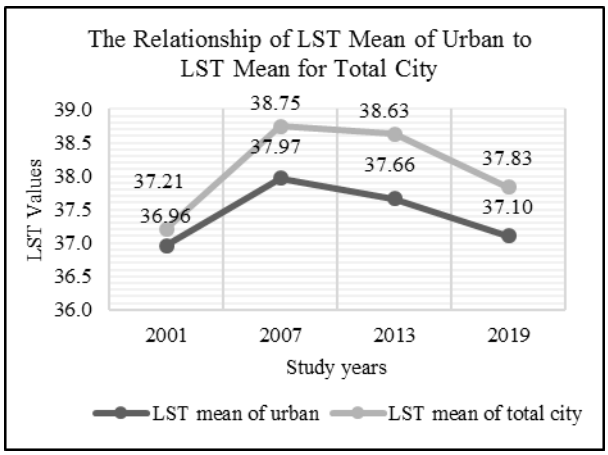

Fig. 13 The relationship of LST mean of urban to LST mean for entire city.

We find that the urban areas and green areas in the new cities constitute cold islands in relation to the desert areas around them. This was confirmed by a study (Walid Abbas Abdel Radi 2013) of the Cairo Complex, in which it was explained that urban areas form cold islands in relation to their desert back, forming what is known as the inverted thermal island. Whereas the urban areas themselves in the Cairo complex constitute positive heat islands in relation to their agricultural back [36]. In the study (Mansour Hussein Salem Saleh 2015) in which he studied the urban climate of the city of Giza, it was explained that the difference in temperature between the city and its rural back decreases from 1984 to 2014. But this decrease was not a result of the decrease in temperatures of the city and the disappearance of the heat island, but rather was as a result of urban sprawl on these agricultural lands, which led to raising their temperatures. While the temperature difference between the city of Giza and its desert hinterland did not differ much during that period [37].

What this means is that the heat island becomes clear depending on the location of the city and its surroundings. The urban areas and green areas in the new cities represent lower temperatures in relation to the empty desert areas around them. But it is necessary to achieve the limits of thermal equilibrium for the body, which was clarified by the study (Mansour 2016), which is that the temperature should not exceed 40℃ as a maximum and not be less than 26℃ as a minimum [38]. Looking at the average temperatures for urbanization in **Fig. 13**, we find that they have achieved this thermal balance over the years of study. The maximum average temperature for urbanization was 38.75℃ in 2007, and the lowest average temperature for urbanization was 37.21℃ in 2001.

4 Conclusion

Increases in LST lead to worsening effects of UHI and thermal comfort. Given the difficulty of measuring LST over large areas and its high cost to researchers in developing countries, this study adopted a framework using freely available RS data from Landsat satellites and GIS. This methodology can be used by planners in developing countries to study the impact of urban growth on UHI. By testing this framework in studying the impact of urban growth on new cities by applying it to the 6 of October City as a case study, it was concluded that urban growth does not pose a threat to the UHI in new cities because they are built in desert cities. Rather, urban growth is lowering LST than it is around it.

With urban growth, the average LST of the entire city decreases, except for the first period (2001 to 2007) when the average LST of the city increased by 1℃, with an increase in the urban area of 8.4%. In the second period (2007 to 2013), the average city LST decreased by 0.3℃, while the urban area increased by 5.7%. Also in the third period (2013 to 2019) the average city LST decreased by 0.5℃, while urban areas increased by 7.9%. This decrease in the average LST, despite the urban growth, is due to increased opportunities for shading and an increase in the presence of green spaces, rather than desert areas that absorb the largest amount of radiation. Thus, the framework has succeeded in providing satisfactory results on the impact of urban growth on UHI. Regardless of the LST values themselves and how they relate to reality, do they need correction or not? But he presented an idea of its connection with urban growth.

References

[1] Omar Hamdy, Shichen Zhao, Taher Osman, Mohamed A. Salheen, and Y. Y. Eid, "Applying a Hybrid Model of Markov Chain and Logistic Regression to Identify Future Urban Sprawl in Abouelreesh, Aswan: A Case Study," Geosciences, vol. 6, no. 4, p. 43, Oct. 2016, doi: 10.3390/geosciences6040043.

[2] Omar Hamdy and Shichen Zhao, "A Study On Urban Growth In Torrent Risk Areas In Aswan, Egypt," J. Archit. Plan. (Transactions AIJ), vol. 81, no. 726, pp. 1733–1741, 2016, doi: 10.3130/aija.81.1733.

[3] Mohamed Mohamed Amin Abd-Allah, "Modelling Urban Dynamics Using Geographic Information Systems, Remote Sensing And Urban Growth Models," no. September, 2007.

[4] Esraa Osama Salem and Miran Essam Monir, "Policies, Strategies, and Mechanisms of New Cities in Egypt," Acad. Res. Community Publ., vol. 1, no. 1, p. 16, Sep. 2017, doi: 10.21625/archive.v1i1.115.

[5] Ibrahim Rizk Hegazy and Wael Seddik Moustafa, "Toward revitalization of new towns in Egypt case study: Sixth of October," Int. J. Sustain. Built Environ., vol. 2, no. 1, pp. 10–18, 2013, doi: 10.1016/j.ijsbe.2013.07.002.

[6] Rizwan Ahmed Memon, Dennis Y.C. Leung, and Liu Chunho, "A Review on the Generation, Determination and Mitigation of Urban Heat Island," J. Environ. Sci., vol. 20, pp. 120–128, 2008.

[7] Duy X. Tran, Filiberto Pla, Pedro Latorre-Carmona, Soe W. Myint, Mario Caetano, and Hoan V. Kieu, "Characterizing the relationship between land use land cover change and land surface temperature," ISPRS J. Photogramm. Remote Sens., vol. 124, pp. 119–132, Feb. 2017, doi: 10.1016/j.isprsjprs.2017.01.001.

[8] Hicham Bahi, Hicham Mastouri, and Hassan Radoine, "Review of methods for retrieving urban heat islands," Mater. Today Proc., vol. 27, pp. 3004–3009, 2020, doi: 10.1016/j.matpr.2020.03.272.

[9] Elham Shafiee, Mohsen Faizi, Seyed-Abbas Yazdanfar, and Mohammad-Ali Khanmohammadi, "Assessment of the effect of living wall systems on the improvement of the urban heat island phenomenon," Build. Environ., vol. 181, p. 106923, Aug. 2020, doi: 10.1016/j.buildenv.2020.106923.

[10] J.A. Voogt and T. R. Oke, "Thermal remote sensing of urban climates," Remote Sens. Environ., vol. 86, no. 3, pp. 370–384, Aug. 2003, doi: 10.1016/S0034-4257(03)00079-8.

[11] Terence Darlington Mushore, John Odindi, Timothy Dube, and Onisimo Mutanga, "Understanding the relationship between urban outdoor temperatures and indoor air-conditioning energy demand in Zimbabwe," Sustain. Cities Soc., vol. 34, no. April, pp. 97–108, Oct. 2017, doi: 10.1016/j.scs.2017.06.007.

[12] Daniela Stroppiana, Massimo Antoninetti, and Pietro Alessandro Brivio, "Seasonality of MODIS LST over Southern Italy and correlation with land cover, topography and solar radiation," Eur. J. Remote Sens., vol. 47, no. 1, pp. 133–152, Jan. 2014, doi: 10.5721/EuJRS20144709.

[13] Qihao Weng, "Thermal infrared remote sensing for urban climate and environmental studies: Methods, applications, and trends," ISPRS J. Photogramm. Remote Sens., vol. 64, no. 4, pp. 335–344, Jul. 2009, doi: 10.1016/j.isprsjprs.2009.03.007.

[14] L. Gadrani, G. Lominadze, and M. Tsitsagi, "F assessment of landuse/landcover (LULC) change of Tbilisi and surrounding area using remote sensing (RS) and GIS," Ann. Agrar. Sci., vol. 16, no. 2, pp. 163–169, Jun. 2018, doi: 10.1016/j.aasci.2018.02.005.

[15] World Meteorological Organization, "WMO Statement on the status of the global climate in 2013," 2014.

[16] T.T. Werner, Anthony Bebbington, and Gillian Gregory, "Assessing impacts of mining: Recent contributions from GIS and remote sensing," Extr. Ind. Soc., vol. 6, no. 3, pp. 993–1012, Jul. 2019, doi: 10.1016/j.exis.2019.06.011.

[17] Sheriza Mohd Razali and Ahmad Ainuddin Nuruddin, "A method of mapping forest fuel types in peat swamp forest," African J. Agric. Res., vol. 7, no. 12, Mar. 2012, doi: 10.5897/AJAR11.1456.

[18] Zeinab Alsonny, Abdel Monteleb Mohammad Ali Ahmed, and Omar Hamdy, "Studying the Effect of Urban Green Spaces Location on Urban Heat Island in Cities Using Remote Sensing Techniques, 6th October City as a Case Study," Int. Des. J., vol. 12, no. 2, pp. 243–262, 2022, [Online]. Available: https://idj.journals.ekb.eg/article_222645.html%0Ahttps://idj.journals.ekb.eg/article_222645_dc463e365fc4bbf3f6719f2316435241.pdf.

[19] Mohamed R. Ibrahim and Houshmand E. Masoumi, "Will Distance to the Capital City Matter When Supplying New Cities in Egypt?," GeoScape, vol. 10, no. 2, pp. 35–52, 2016, doi: 10.1515/geosc-2016-0004.

[20] The electronic portal of 6th October City development authority, "Land uses for the city of 6th October," 2013. http://www.6october.gov.eg/pages/.aspx (accessed May 02, 2021).

[21] Mohamed Mahmoud Abdullah Youssef, "Optimal use of land and sustainable development by applying to the Sixth of October City in Egypt," Organ. Islam. Capitals Cities, 2013.

[22] Walid Abbas Abdel Radi Hassan, "The intensity of the heat islands of the main cities in the Nile Delta, a comparative study in the urban climate using Terra MODIS visuals," Ann. Fac. Arts, Ain Shams Univ., vol. 44, no. July-September (c), pp. 373–411, Sep. 2016, doi: 10.21608/aafu.2016.9684.

[23] "EarthExplorer." https://earthexplorer.usgs.gov/ (accessed Aug. 25, 2021).

[24] Omar Hamdy, "Using Remote Sensing Techniques to Assess the Changes in the Rate of Urban Green Spaces in Egypt: A Case Study of Greater Cairo," Int. Des. J., vol. 12, no. 3, pp. 53–64, 2022.

[25] Stephen V. Stehman, "Estimating the kappa coefficient and its variance under stratified random sampling," Photogramm. Eng. Remote Sensing, vol. 62, no. 4, pp. 401–407, 1996.

[26] Felicien Nkomeje, "Comparative Performance of Multi-Source Reference Data to Assess the Accuracy of Classified Remotely Sensed Imagery: Example of Landsat 8 OLI Across Kigali City-Rwanda," Int. J. Eng. Work. Kambohwell Publ. Enterp., vol. 4, no. 1, pp. 10–20, 2015, doi: https://doi.org/10.5281/ZENODO.268398.

[27] M. Noby, U. Michitaka, and O. Hamdy, "Urban Risk Assessments: Framework for Identifying Land-uses Exposure of Coastal Cities to Sea Level Rise, a Case Study of Alexandria," SVU-International J. Eng. Sci. Appl., vol. 3, no. 1, pp. 78–90, 2022, doi: 10.21608/svusrc.2022.132215.1045.

[28] M.A. Kalkhan, Robin M. Reich, and Raymond L., "Variance Estimates and Confidence Intervals for the Kappa Measure of Classification Accuracy," Can. J. Remote Sens., vol. 23, no. 3, pp. 210–216, Sep. 1997, doi:

10.1080/07038992.1997.10855203.

[29] O. Hamdy and Z. Alsonny, “Assessing the Impacts of Land Use Diversity on Urban Heat Island in New Cities in Egypt, Tiba City as a Case Study,” Int. Des. J., vol. 12, no. 3, pp. 93–103, 2022.

[30] Abdu Yaro, Lawal Abdulrashid, Jerome Ayodele John, and Yahaya Sani, “Remote Sensing and GIS Based Assessment of Urban Heat Island Pattern in Remote Sensing and GIS Based Assessment of Urban Heat Island Pattern in Kaduna Metropolis,” Int. J. Res. Appl. Nat. Sci., vol. 3, no. 6, 2017.

[31] Ali Asgarian, Bahman Jabbarian Amiri, and Yousef Sakieh, “Assessing the effect of green cover spatial patterns on urban land surface temperature using landscape metrics approach,” Urban Ecosyst., vol. 18, no. 1, pp. 209–222, Mar. 2015, doi: 10.1007/s11252-014-0387-7.

[32] M. B. Giannini, O. R. Belfiore, C. Parente, and R. Santamaria, “Land Surface Temperature from Landsat 5 TM images: comparison of different methods using airborne thermal data,” J. Eng. Sci. Technol. Rev., vol. 8, no. 3, pp. 83–90, Jun. 2015, doi: 10.25103/jestr.083.12.

[33] Samer Hadi Kazem Al-Jashmi, “Spatial analysis of heat islands in the city of Najaf using geographical techniques,” J. Geogr. Res., vol. 27, no. 1, p. 327, 2018, doi: 10.36328/0833-000-027-012.

[34] Xiaolei Yu, Xulin Guo, and Zhaocong Wu, “Land Surface Temperature Retrieval from Landsat 8 TIRS—Comparison between Radiative Transfer Equation-Based Method, Split Window Algorithm and Single Channel Method,” Remote Sens., vol. 6, no. 10, pp. 9829–9852, Oct. 2014, doi: 10.3390/rs6109829.

[35] Aliihsan Sekertekin and Stefania Bonafoni, “Land Surface Temperature Retrieval from Landsat 5, 7, and 8 over Rural Areas: Assessment of Different Retrieval Algorithms and Emissivity Models and Toolbox Implementation,” Remote Sens., vol. 12, no. 2, p. 294, Jan. 2020, doi: 10.3390/rs12020294.

[36] Walid Abbas Abdel Radi, “The temperature in the Cairo urban complex,” 2013.

[37] Mansour Hussein Salem Saleh, “The urban climate of Giza city using remote sensing and GIS.,” 2015.

[38] Kamel Fathy Gomaa Mansour, “Studying the relationship between urban changes and the emergence of heat islands in the city of Tanta using remote sensing and geographic information systems,” J. Sci. Res. Arts, vol. 3, no. 4, pp. 1–18, Aug. 2016, doi: 10.21608/jssa.2016.11381.